TDMA in Adaptive Resonant Beam Charging for IoT Devices

Mingliang Xiong, Mingqing Liu, Qingqing Zhang, *Student Member, IEEE*,
Qingwen Liu⬤ , *Senior Member, IEEE*, Jun Wu⬤ , *Senior Member, IEEE*, and Pengfei Xia⬤

Abstract—Resonant beam charging (RBC) can realize wireless power transfer (WPT) from a transmitter to multiple Internet of Things devices via resonant beams. The adaptive RBC (ARBC) can effectively improve its energy utilization. In order to support multiuser WPT in the ARBC system, we propose the time-division multiple access (TDMA) method and design the TDMA-based WPT scheduling algorithm. Our TDMA WPT method has the features of concurrently charging, continuous charging current, individual user power control, constant driving power, and flexible driving power control. The simulation shows that the TDMA scheduling algorithm has high efficiency, as the total charging time is roughly half (46.9% when charging 50 receivers) of that of the alternative scheduling algorithm. Furthermore, the TDMA for WPT inspires the ideas of enhancing the ARBC system, such as flow control and quality of service.

Index Terms—Internet of Things (IoT), resonant beam charging (RBC), time-division multiple access (TDMA), wireless power transfer (WPT).

I. Introduction

WIRELESS power transfer (WPT) becomes an important and urgent need for mobile devices, such as smartphones [1] and Internet of Things (IoT) devices [2], [3]. Recently, Qihui Wu and Guoru Ding have made the primary contributions to cognitive Internet of things (CIoT) and its applications, which provided valuable references for this work [4], [5]. For the emerging area of CIoT, a high-power and human-safe WPT can promote the massive data acquisition and analysis of CIoT devices. WPT, as known as wireless charging, can be classified into nonradiative coupling-based charging and radiative radio frequency-based charging [6]. In terms of power transmission distance, wireless charging can be classified into far-field charging and near-field charging [7]. The WPT technologies, such as inductive coupling [8], magnetic resonance coupling [9], [10], capacitive coupling [11], radio waves [12], and laser [13], have been well investigated in researches. However, these WPT technologies are facing various technical challenges. For instance, inductive coupling has to operate in short-distance; radio-wave charging suffers
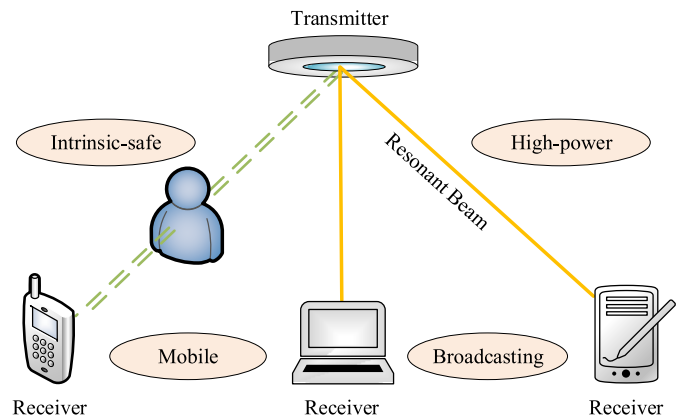

Fig. 1. RBC features.

low efficiency; and laser charging has the difficulty to meet the safety requirements.

Resonant beam charging (RBC), as known as distributed laser charging [14], can transfer energy via a resonant beam between the transmitter and the receiver. Fig. 1 shows the RBC features including high-power, intrinsic-safe, mobile, and broadcasting. RBC can safely charge multiple moving devices with Watt-level power over meter-level distances like WiFi communications. The adaptive RBC (ARBC) system proposed in [15] improved the WPT efficiency based on feedback control like link adaptation in wireless communications.

Although single-user ARBC was presented in [15], multiuser WPT in the ARBC system is important and worth of investigating for the applications like wireless sensor networks [16]–[18]. Thus, multiple access in the ARBC system needs to be studied. Furthermore, it is also interesting to find out an efficient scheduling method for multiuser WPT in the ARBC system, in order to satisfy each user's energy requirement.

In this paper, we propose two types of power control methods for the multiuser ARBC system: 1) the alternative charging and 2) the time-division multiple access (TDMA) charging.

Alternative Charging: The transmitter transfers proper power to one receiver for a period of time and then switches to another. However, this design has two obvious limitations: 1) the efficiency is low as only one receiver can be charged in each charging period and 2) charging current may be discontinuous due to user switch.

TDMA Charging: It combines time-division multiplexing (TDM) and pulse width modulation (PWM) for multiuser

WPT, which has neither of the above limitations. In communication systems, TDM was originally introduced to combine multiple signals in one channel in time domain [19]. Then, TDM was adopted for WPT as TDM-WPT in [20]. PWM technology provides an approach to convert pulses into continuous current, which is widely adopted in switching mode power supply (SMPS) [21]. We employ TDM to handle multiuser WPT and employ PWM to realize continuous current charging.

The contribution of this paper includes: 1) we design and analyze the PWM-assisted TDMA method for multiuser WPT in the ARBC system and 2) we propose the TDMA-based scheduling algorithm to realize efficient and flexible multiuser WPT in the ARBC system. The proposed TDMA-based charging design has the following features.

1) *Concurrently Charging:* Multiple receivers can be charged concurrently.
2) *Individual User Power Control:* The charging power of each receiver can be controlled independently.
3) *Continuous Charging Current:* The charging current of each receiver is continuous.
4) *Constant Driving Power:* The driving power at the transmitter can keep constant and avoid being frequently switched as in alternative charging, which leads to low-complexity and robustness for the transmitter design.
5) *Flexible Driving Power Control:* The driving power can be flexible regardless of charging power requirements.

Compared with the alternative charging method, the TDMA-based method has the following benefits.

1) *Charging Efficiency:* The total charging time for multiple users is 46.9% of that of the alternative charging.
2) *Output Capability:* There is no limit on output power.
3) *User Capacity:* The system can support more users due to the improvement of output capability.

In Section II, we introduce the principle of RBC; present the point-to-point ARBC system; depict the multiuser charging problem in the ARBC system; and demonstrate the alternative charging method. In Section III, we propose the TDMA method for multiuser WPT in the ARBC system. In Section IV, we depict the TDMA-based scheduling algorithm. In Section V, we illustrate the simulation to compare the efficiency between the alternative and TDMA-based charging methods, and summarize the features of the TDMA-based scheduling algorithm. Finally, in Section VI, we make the conclusions and discuss the future research topics.

II. SYSTEM DESCRIPTION

In this section, we first introduce the principle of RBC. Then, we depict the point-to-point ARBC system which supports the TDMA charging in Section III. Next, we demonstrate the necessity of multiuser power control when charging multiple receivers. At last, we propose the alternative scheduling algorithm and discuss its features.

A. Resonant Beam Charging

As shown in Fig. 2, the RBC system consists of two parts: 1) the transmitter and 2) the receiver. In the system,
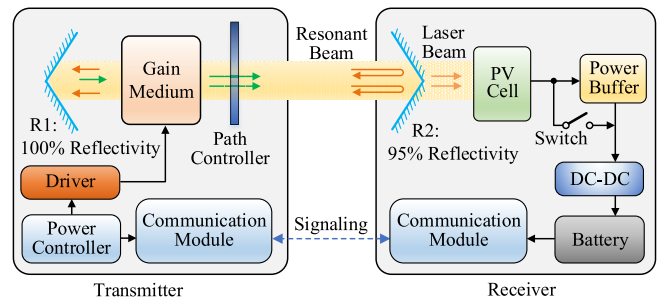

Fig. 2.   ARBC system.

the transmitter and the receiver constitute the resonant cavity. Therefore, differing from the traditional laser cavity, the RBC cavity is separated in space. R1 and R2 are retro-reflectors, which can reflect the beam to the reverse direction regardless of the incident angle [22]. Between the two retro-reflectors, the photons are reflected repeatedly to stimulate out more photons while passing through the gain medium. Hence, the resonant beam connecting R1 and R2 can be formed naturally without concerning about the location of the receiver. The above mechanism guarantees the features of mobility and broadcasting. As a retro-reflector with 95% reflective, R2 allows a part of the photons passing through. Therefore, a laser beam can output from the back of R2, which can provide high-power energy. Furthermore, any obstacles such as human bodies and clothes that enter the resonating beam path will disrupt the resonance immediately, which provides the intrinsic safety. At last, the beam can be converted into current by the photovoltaic (PV) cell to charge the battery.

B. Point-to-Point System

The point-to-point system is depicted in Fig. 2. In the transmitter, the driver provides the driving power for the gain medium to generate the beam. This process converts electrical energy into optical energy. Then, the beam travels through the air, resonating between the transmitter and the receiver. The path controller is composed of an optical switches array, and it is adopted to switch the on–off state of the beam path. In the receiver, the PV cell converts optical energy into electrical energy. As the most important element for the implementation of the TDMA charging method, the power buffer can convert PWM power into continuous smooth power. However, for the alternative charging, the power buffer should be bypassed by closing the switch. The direct current to direct current (dc–dc) converter ensures that the charging voltage and the charging current can satisfy the battery's requirement. The communication modules can transmit battery states from the receiver to the transmitter via the signaling channel. At the transmitter, the power controller can control the driving power.

In the system model, the electrical energy provided by the driver is converted into optical energy with the efficiency η_s. The transmission efficiency of the path controller is η_{pc}. Due to propagation attenuation, the resonant beam power experiences power loss with the transmission efficiency η_t. Moreover, the photoelectric conversion efficiency of the PV cell is η_r. The
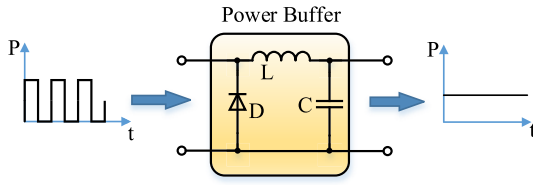
Fig. 3.   Power buffer principle.

conversion efficiency of the power buffer is η_{pb}. The conversion efficiency of the dc–dc converter is η_{dc}. We define the driving power as P_d, then the charging power P_c can be obtained as

$$P_c = \eta_s \eta_{pc} \eta_t \eta_r \eta_{pb} \eta_{dc} P_d. \tag{1}$$

The principle of the power buffer is depicted in Fig. 3. The PWM wave is input to the power buffer, and the output is the continuous current. The circuit of the power buffer is similar to that of an SMPS, which consists of the energy storage components such as inductors and capacitors [23]. Inductors have the ability to store electrical energy by converting it into magnetic energy. Similarly, capacitors store electrical energy in the form of electric charges. As pulses enter the power buffer, the analysis can be divided into two stages.

1) *ON Stage:* The input power of the power buffer is at a high level, which is notated as the peak input power P_{bip}; and the diode remains a cut-off state while the capacitor is being charged by the inductor. As a result, the output voltage rises up slowly.

2) *OFF Stage:* Following the ON stage, the input power turns to zero, and the diode is switched on. Thus, the energy stored in the inductor is released to the capacitor and the load. Therefore, the output voltage goes down slowly.

In theory, there is no energy consumption in such components as inductors and capacitors without resistance. Because of the law of energy conservation in a period

$$E_{bo} = E_{bi} \tag{2}$$

it can be induced that

$$P_{bo} T_w = P_{bip} \cdot T_{ON} + 0 \times (T_w - T_{ON}) \tag{3}$$

where E_{bi} is the input energy, E_{bo} is the output energy, P_{bip} is the peak power of the input pulse, P_{bo} is the constant output power, T_{ON} is the time width of the pulse (ON stage), and T_w is the period of the PWM wave. The duty cycle δ of the PWM wave is depicted as

$$\delta = \frac{T_{ON}}{T_w}. \tag{4}$$

Hence, from (3) and (4), it can be derived that

$$P_{bo} = \delta P_{bip}. \tag{5}$$

Then, from (1) and (5), the charging power can be obtained as

$$P_c = \eta \delta P_d \tag{6}$$

where

$$\eta = \eta_s \eta_{pc} \eta_t \eta_r \eta_{pb} \eta_{dc}. \tag{7}$$
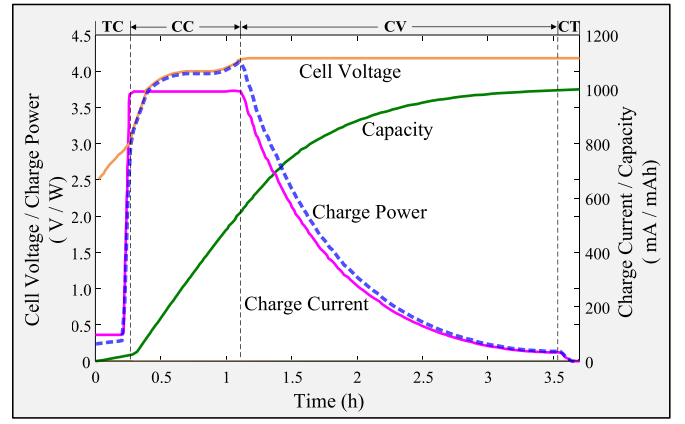

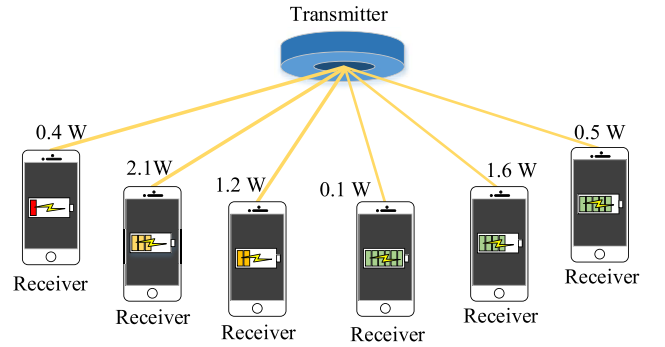Fig. 4.   Li-ion battery charging profile.

Fig. 5.   Multiuser power control.

From (6), we can verify that the charging power can be determined by the duty cycle of the PWM beam.

C. Multiuser Power Control

RBC has the broadcasting feature, as the resonant beams can be formed between one transmitter and multiple receivers. However, the broadcast charging is less efficient in energy utilization, because the RBC system cannot track the receivers' power requirements concurrently.

Owing to the advantages of high energy density and long cycling life, Li-ion batteries are the most common energy storage components in mobile devices. The specified constant current–constant voltage (CC–CV) charging algorithm can optimize the battery performance [24]. The CC–CV algorithm can be depicted in Fig. 4 which is called the Li-ion battery charging profile. The charging profile has four stages in a charge circle, which are trickle charge, constant current (CC), constant voltage (CV), and charge terminal, respectively [24].

According to the CC–CV algorithm, the battery is charged with the dynamic power in the ARBC system. From Fig. 4, when charging the 1000 mAh Li-ion battery, the charging power rises up from zero to the maximum value (4.2 W) and then goes back to zero smoothly. Hence, each receiver has a unique desired charging power P_c according to the charging profile during the charging period. As shown in Fig. 5, the charging power delivered to each receiver should be specified. In order to optimize each receiver's battery performance, the charging power per receiver should be controlled according to
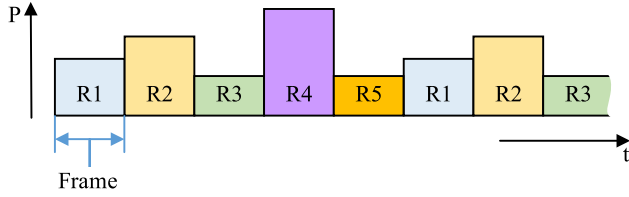
Fig. 6.   Alternative charging principle.

Fig. 7.   Time-division multiple accessing charging principle.

its battery charging profile. Therefore, how to realize multiuser power control in the ARBC system to track the receivers' requirements concurrently becomes an important issue.

D. Alternative Charging

In order to realize multiuser power control, the alternative charging is an intuitive method without the power buffer (i.e., the switch is closed in Fig. 2). In Fig. 6, time is divided into a sequence of small frames with the same width. In each frame, the transmitter generates a beam for only one receiver (R1, R2, R3, R4, or R5) sequentially with the receiver's battery desired charging power. This charging procedure (charging from R1 to R5 in turns) will repeat until all the receivers are fully charged. Thus, the scheduling algorithm can be depicted as follows.

Alternative Scheduling Algorithm: To charge the receivers sequentially with their desired battery charging power, repeatedly, and removes those receivers whose capacity reaches to 100%.

However, after being charged in one frame, the receiver have to wait for its next charging frame in a long time (e.g., four frames in Fig. 6). Therefore, the alternative charging has the disadvantages of low efficiency and discontinuous battery charging current.

The driving power at the transmitter is switched over a frame. The frequent driving power adjustment may be harmful for the gain medium and lead to the complex transmitter design. Moreover, the driving power is constrained to satisfy only one receiver's requirement per frame, which is inflexible and leads to the restricted output capability. To solve those problems, a more efficient and flexible multiple access method will be proposed in the next section.

III. TDMA CHARGING DESIGN

In this section, we propose the TDMA charging design in the ARBC system, which have the features of currently multiuser charging, individual user power control and continuous charging current. We at first demonstrate the TDMA charging principle. Then, we propose the digitalized design to facilitate the computer control.

A. TDMA Charging Principle

With the system illustrated in Section II, the transmitter should send the ON–OFF alternative PWM beam to the receiver, and the charging power can be determined by the duty circle (pulse width) of the PWM beam. The pulse takes only two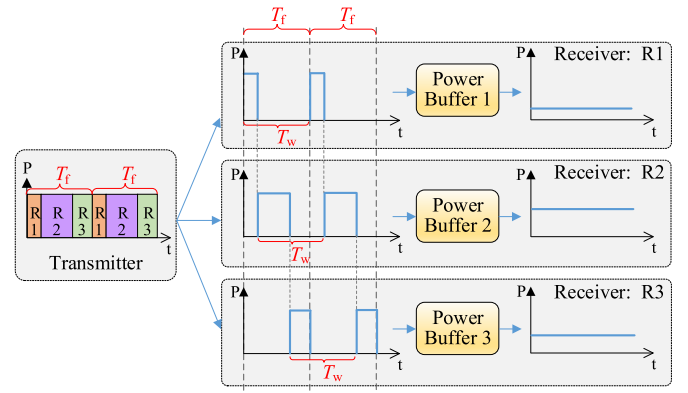 stages: 1) the ON stage and 2) the OFF stage. During the ON stage, the transmitter opens the path for the beam orientating to one receiver, and closes during the corresponding OFF stage. In the OFF stage the transmitter is idle without energy output. If the second receiver's ON stage duration is shorter than the first receiver's idle time (the OFF duration), the transmitter could send the beam pulse to the second receiver in the first receiver's idle time, in order to improve the time utilization.

Based on the above idea, we can borrow the TDMA principle to combine multiple beam pulses in one frame. In Fig. 7, in a frame period T_f, the transmitter generates three beam pulses one-by-one to three receivers (R1, R2, and R3) with different pulse width for each receiver. Then, in the following frames, the transmitter repeats this beam pulses pattern. As a result, from each receiver's perspective, a PWM wave with the period of T_w is received and eventually converted by the power buffer to a continuous power. However, from the transmitter's point of view, it sends three PWM beams to three receivers. These PWM beams take the same fixed transmitting power and the same period T_w with different pulse width per receiver. Because the pulse widths of the three PWM beams are different, the output powers from the power buffers are distinct. Actually, the width of a frame is equal to the period of each PWM beam, namely,

$$T_w = T_f. \tag{8}$$

From (6), the transmitter can calculate the desired duty circle δ for each receiver according to its desired charging power P_c (as shown in Fig. 4). If δ and T_w are determined, the desired pulse width T_{ON} can be obtained from (4). Then, N_c receivers can be selected to form a frame, according to the *selecting rule* that the sum of these receivers' desired pulse widths must be less than a frame time

$$\sum_{i=0}^{N_c} T_{ON_i} \le T_f \tag{9}$$

where T_{ON_i} is the time width of the pulse sent to the ith selected receiver.

The transmitter can send beam pulses to each selected receiver with corresponding pulse width and order, and all of the selected receivers can obtain continuous smooth current concurrently.
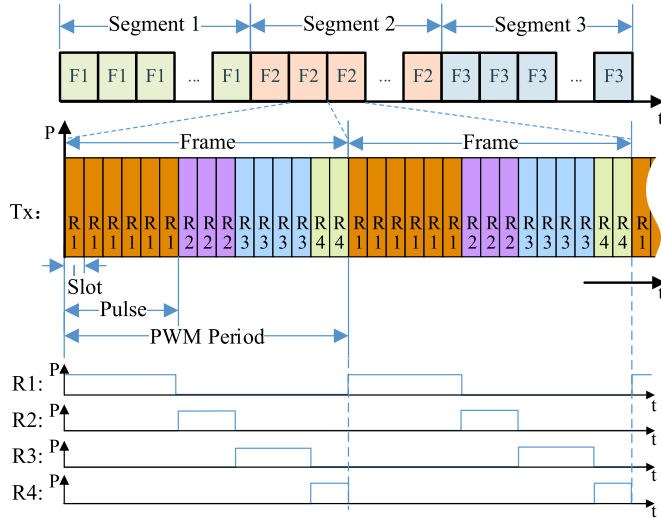
Fig. 8. Digitalized TDMA charging design.

B. Digitalized TDMA Charging Design

The TDMA charging is to combine the PWM pulses for the selected receivers in a frame. In order to adopt the computer control in the TDMA charging, we design the digitalized rule which contains three structures: 1) segment; 2) frame; and 3) slot.

Fig. 8 shows the digitalized TDMA charging design. The time is divided into a number of segments. Each segment contains several identical frames. Each frame is divided into a number of slots. The slots are the identical time units and can be allocated to some proper receivers. For example, in Fig. 8, the notations R1, R2, R3, and R4 represent the receivers. If one slot is allocated to a receiver, then the transmitter can generate the beam to this receiver in this time slot. In Fig. 8, the adjacent slots with the same receiver notation constitute this receiver's pulse. The pulses marked with the same receiver notation constitute a PWM that will be sent to the corresponding receiver. The peak power of these pulses is constant. For instance, in Fig. 8, the first six slots in each frame F2 are marked as R1, so the transmitter Tx will switch the beam orientating to the receiver R1 during those time slots, as a result, R1 will receive a PWM wave whose pulse width and period is equal to 6 slots and 15 slots, respectively.

All of the slots have the same time width T_s. The time width of each frame is T_f. Hence, the total slot number, N_s, in one frame can be obtained as

$$N_s = \frac{T_f}{T_s}. \tag{10}$$

For instance, Fig. 8 shows the details of the frame F2 which is divided into $N_s = 15$ slots.

As the peak power, P_p, of the pulse beam is constant, the driving power P_d in ON stage can also be a fixed value. However, the desired charging powers, P_c, of the receivers are distinct. From (6), given the value of P_c, the desired PWM duty cycle δ can be induced as

$$\delta = \frac{P_c}{\eta P_d}. \tag{11}$$

In order to form a pulse for a specific receiver with a desired width, the transmitter needs to allocate the desired number of slots to the receiver. The desired slot number N_c can be induced as

$$N_c = \lceil \delta N_s \rceil = \left\lceil \frac{P_c}{\eta P_d} N_s \right\rceil \tag{12}$$

where the ceiling notation is used to ensure that N_c is the proper integer which can provide enough energy for the receiver. For example, in Fig. 8, N_c of the receivers from R1 to R4 are 6, 3, 4, and 2, respectively.

Segment is a period of time T_g, consisting of consecutive identical frames. However, the frames in different segments may not be identical. For example, in Fig. 8, segment 1 consists of several frames F1, while in segment 2 the frames are F2.

The structure of segments is important in the design. The pulses for multiple receivers are arranged closely in a frame to ensure the optimal time distribution. If the pulse width of one receiver increases, the pulses of other receivers in the same frame must move their positions backward, which brings an unpredictable situation that the last pulse in the fame may have no enough place. To avoid the unpredictable situation, the pulse width of each PWM wave must be constant, and the position of each pulse in the frame must be fixed. Therefore, the segment structure should contain several identical frames to provide a long period of time for stably outputting PWM waves.

In summary, the segment structure ensures the selected receivers to be charged continuously for an effective long duration. The segment is an important term in the *OUTPUTTING* procedure of the TDMA scheduling algorithm, which will be specified in Section IV.

The above multiplexing of PWM waves leads to the concurrently charging feature. Hence, we define the following.

Multiplexing Number: ψ, as the number of the selected receivers in a frame.

For instance, in Fig. 8, ψ of frame F2 is 4, because four receivers are contained in the frame. We define the average multiplexing number, Ψ, of a charging process as

$$\Psi = \sum_{0 \leq t_i < T_u} \frac{\psi_i T_f}{T_u}, \quad i = 1, 2, 3, \ldots, n \tag{13}$$

where ψ_i is the multiplexing number of the *i*th frame, t_i is the time when starting to handle the *i*th frame, and T_u is the

In summary, the TDMA charging originates from the concepts combination of TDM and PWM. The advantages includes the following three aspects.

1) Multiple receivers can be charged with different charging power continuously and concurrently.
2) The transmitter generates beams to receivers with the same driving power.
3) The driving power can be customized to an desired value flexibly.

Fig. 9.   Flow chart of TDMA charging algorithm.

TABLE I
DEVICE PROFILE STRUCTURE

Parameter	Description
C_r	residual battery capacity
P_c	desired charging power
N_c	desired slot number
...	other parameters: ID, location, etc.

TABLE II
DATA NOTATION DEFINITIONS

Notation	Type	Description
$\mathbf{m}[\ ]$	device profile array	receivers to be accessed
$\mathbf{S}[\ ]$	device profile array	accessed receivers
$\mathbf{F}[\ ]$	device profile array	slot allocation
t	timer	counting the time
N_s	constant	slot number per frame
P_d	constant	driving power
T_s	constant	slot width
T_g	constant	segment width
C_{full}	constant	full battery capacity

time costed in the total charging process. The value of Ψ can be used to evaluate the efficiency of the TDMA scheduling algorithm.

In summary, the transmitter can control the charging power for each receiver by controlling the slot number allocated to the receiver. Therefore, the transmitter can switch the beam orientation toward the receiver according to its allocated slots in a frame. Based on the repeated frame structure per segment, the PWM wave can be obtained per receiver. Finally, relying on the power buffer, the receiver can be charged with continuous and smooth current.

IV. TDMA-BASED SCHEDULING ALGORITHM

The above sections introduce the hardware requirements and the TDMA charging design. In this section, we will introduce the TDMA-based scheduling algorithm, which contains the rule of slots allocation and provides a logical scheduling procedure. In summary, we define the following.

TDMA Scheduling Algorithm: To allocate slots to the receivers according to their desired charging power and residual battery capacity; then, form the frame structure, and operate a segment in a scheduling period.

As is depicted in Fig. 9, we divide the TDMA scheduling algorithm into the following five parts.

1) *ACCESSING:* To send acknowledgments to the receivers after receiving the requests; then handle authentications and record the information of the accessed receivers.
2) *REFRESHING:* To obtain the battery states of the receivers, such as residual battery capacity and desired charging power, via the signaling channels; and calculate the desired slots number of the receivers.

3) *FILTERING:* To remove the information of the full-capacity receivers from the memory to ensure that those receivers are no longer charged.
4) *ALLOCATING:* To sort receivers according to the residual battery capacity in ascending order; select some receivers with proper rules; and form a frame by allocating slots to the selected receivers.
5) *OUTPUTTING:* To operate a segment of charging by running a loop, where the transmitter output beams according to the frames with a constant driving power.

The pseudocode of the TDMA scheduling algorithm is listed in Algorithm 1. We first introduce the data structure of the device profile, which records the information of the receiver. The parameters in the device profile structure are listed in Table I. The notation definitions of the data in the algorithm are listed in Table II. In the pseudocode, a pair of square brackets wrapping up a number (i, for example) after a symbol means an element (the ith element, for example) of the array that marked by the symbol.

In the *ACCESSING* procedure (steps 2–6 in Algorithm 1), there are N receivers waiting for connection. The transmitter handles the requests from the receivers $\mathbf{m}[i]$, ($i = 1, 2, 3, \ldots, N$). If one receiver succeeds in authentication, a connection will be created and the device profile will be recorded as an element in the array $\mathbf{S}$. The instruction *append* $\mathbf{m}[i]$ *to* $\mathbf{S}$ means adding an element which is a copy of $\mathbf{m}[i]$ to the tail of $\mathbf{S}$.

In the *REFRESHING* procedure (steps 7–14 in Algorithm 1), the instruction *refreshing* indicates that the transmitter sends notifications to the receivers in the array $\mathbf{S}$ and then collects the battery states returned via the signaling channels. One parameter of the battery state is the residual

Algorithm 1 TDMA Scheduling

1: **begin**
2: **for** $i = 1$ to N **do**
3:     **if** $\mathbf{m}[i]$ is authenticated **then**
4:       *append* $\mathbf{m}[i]$ *to* $\mathbf{S}$
5:     **end if**
6: **end for**
7: **for** $i = 1$ to *length*($\mathbf{S}$) **do**
8:     *refresh* $\mathbf{S}[i].C_\mathrm{r}$ and $\mathbf{S}[i].P_\mathrm{c}$
9:     calculate $\mathbf{S}[i].N_\mathrm{c}$ according to formula (12)
10:    **If** $\mathbf{S}[i].C_\mathrm{r} \geq C_\mathrm{full}$ **then** *delete* $\mathbf{S}[i]$
11: **end for**
12: **if** $\mathbf{S}$ is empty **then**
13:     **end**
14: **end if**
15: sort $\mathbf{S}$ according to $\mathbf{S}. C_\mathrm{r}$ in ascending order
16: **for** $i = 1$ to *length*($\mathbf{S}$) **do**
17:     **if** $\mathbf{S}[i].N_\mathrm{c} \leq N_\mathrm{s} - length(\mathbf{F})$ **then**
18:       **for** $j = 1$ to $\mathbf{S}[i].N_\mathrm{c}$ **do**
19:         *append* $\mathbf{S}[i]$ *to* $\mathbf{F}$
20:       **end for**
21:     **end if**
22: **end for**
23: restart timer t
24: **while** $t \leq T_\mathrm{g}$ **do**
25:     **for** $i = 1$ to *length*($\mathbf{F}$) **do**
26:       output to $\mathbf{F}[i]$ for T_s secs with driving power P_d
27:     **end for**
28:     sleep for $(N_\mathrm{s} - length(\mathbf{F})) \times T_\mathrm{s}$ secs without output
29: **end while**
30: empty $\mathbf{F}$, and **goto** step 7

capacity C_r which implies the urgency level for charging. Another important parameter is the desired charging power P_c which determines the number of the slots that should be allocated. Then, it calculates the desired slot number N_c for each receiver based on (12). All the device profiles of the receivers will be refreshed in this procedure. The instruction length($\mathbf{S}$) represents the number of the elements recorded in $\mathbf{S}$.

In the *FILTERING* procedure (step 10 in Algorithm 1), some of the receivers in the memory will be deleted. Only the devices which are not fully charged (the capacity is less than the maximum capacity C_full) will remain in the array $\mathbf{S}$. The instruction delete $\mathbf{S}[i]$ means removing the ith element of the array $\mathbf{S}$. After the *FILTERING* procedure, if $\mathbf{S}$ is found empty, the scheduling procedure will finish.

The TDMA scheduling algorithm employs the digitalized TDMA charging rule. It divides a frame T_f into the fixed number N_s slots, with the fixed slot time-width T_s. As in Section III, the frame width is equal to the period of the PWM wave. Hence, the frequency of each PWM wave is $1/T_f$. *ALLOCATING* is the procedure to form the frame by allocating the slots in a frame to the selected receivers.

In the *ALLOCATING* procedure (steps 15–22 in Algorithm 1), the array $\mathbf{S}$ is sorted in ascending order

according to the parameters of the residual capacity C_r, which means the receivers with low C_r will be arranged in the front of the array. Then, the allocating procedure begins. An allocating loop is employed to scan the array $\mathbf{S}$ from the head element to the tail. During the scanning, if N_c of the scanned receiver is less than the number of the unallocated slots in the frame (i.e., the condition in (9) is satisfied), the receiver will be selected, and the corresponding slots in the frame will be allocated to this receiver. In a nutshell, the receiver with less residual capacity has the higher priority to be selected.

In the scanning loop, the selected receivers are allocated with proper number of slots which occupy corresponding positions in the array $\mathbf{F}$ (represents a frame), i.e., the elements in $\mathbf{F}$ represent the slots in the frame. If the receiver $\mathbf{S}[i]$ can be allocated with N_c slots, then N_c copies of the device profile recorded in $\mathbf{S}[i]$ will be appended, as the elements, to the tail of $\mathbf{F}$, except for the case that the frame cannot provide enough unallocated slots for the receiver.

In summary, in the *ALLOCATING* procedure, the group of the selected receivers is determined by both C_r and N_c of these receivers. However, the parameters are changed in each *REFRESHING* procedure. Therefore, the number of the selected receivers is not fixed. As a result, the multiplexing number ψ is dynamic during the whole charging process.

At last, in the *OUTPUTTING* procedure (steps 23–30 in Algorithm 1), a timer t is enabled first to count the elapsed time. Then, the procedure executes a charging loop to operate a segment, of which the total loop time is a segment time T_g. Each period of the charging loop operates a frame, i.e., the transmitting beam is generated for the selected receivers from the array $\mathbf{F}$. Therefore, the timing of sending beams is accordance with the elements in $\mathbf{F}$. The transmitter should send beam to the receiver recorded by the element. If the scanning finishes, the procedure will sleep for $(N_s - length(\mathbf{F})) \times T_s$ s (the time of unallocated slots) without output. The sleep operation ensures that the period of the PWM waves equal to the frame width T_f. The operation time of each output or sleep is one slot time T_s. Moreover, the driving power P_d is also a constant value. If the charging loop finishes, all the elements in $\mathbf{F}$ will be deleted, and the procedure will jump to step 7 to start a new scheduling period.

V. Simulation and Analysis

In this section, we introduce the MATLAB simulation of the alternative and TDMA scheduling algorithms. In the analysis, we focus on two aspects: 1) the comparison of the charging efficiency between the two algorithms and 2) the features of the TDMA scheduling algorithm.

A. Simulation Parameters

In Section II, there are several conversion and transmission efficiencies in the ARBC system. The system components of the two scheduling algorithms are identical. We assume:
1) the electro-optical conversion efficiency η_s is 40% [25], [26];
2) the transmission efficiency over the air η_t is 100% [27];

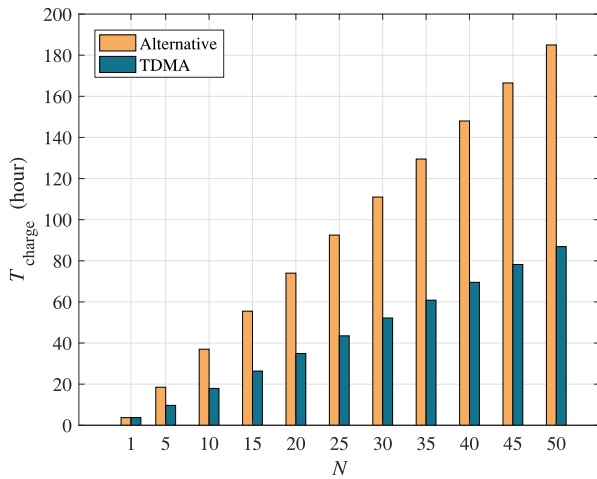Fig. 10.   Charging time T_{charge} versus receiver number N (0 initial residual battery capacity).

Fig. 11.   Charging time T_{charge} versus receiver number N (random initial residual battery capacity).

3) the photoelectric conversion efficiency η_r is 50% (GaAs-based PV cell, 25 °C) [28];

Moreover, we assume η_{pc}, η_{pb}, and η_{dc} are 100%, because the path controller, the power buffer, and the dc–dc converter have less energy consumption [29], [30]. Therefore, the point-to-point charging efficiency η is 20% based on (7). For the alternative scheduling algorithm, the frame time T_f is 0.2 ms. For the TDMA scheduling algorithm, the looping time (one segment) T_g is 1 s; the total slot number of a frame, N_s, is 200; and the frequency of the PWM wave is 5 kHz. Thus, the slot time T_s is 1 μs and the frame time T_f is 0.2 ms. Each receiver is equipped with a single cell Li-ion battery whose maximum capacity is 1000 mAh. The maximum charging power is 4.2 W, as shown in Fig. 4.

B. Algorithm Comparison

In order to compare the efficiency between the TDMA scheduling and the alternative scheduling algorithms. The initial residual capacity of each receiver's battery is set as zero. In the alternative scheduling algorithm, the driving power is dynamic, and its maximum value is 21 W calculated by 4.2 W/20%, where 4.2 W is the maximum charging power according to Fig. 4. For fair comparison, we set the driving power P_d as 21 W for the TDMA scheduling algorithm. To compare the two algorithms quantitatively, we define the following.

Charging Time: T_{charge}, the time duration of charging the battery from the initial residual capacity to full capacity for all accessed receivers.

Fig. 10 shows the variation of T_{charge} with the different receiver number N. The relationship between T_{charge} and N is close to linearity. T_{charge} of the TDMA scheduling algorithm is about half (46.9% when $N = 50$) of that of the alternative scheduling algorithm, except for the special situation where $N = 1$.

In practice, the initial residual capacity should be random rather than zero. We can assume the battery's initial residual capacity is uniformly distributed. In order to minimized the impact of randomness, the simulation runs for 10 times to
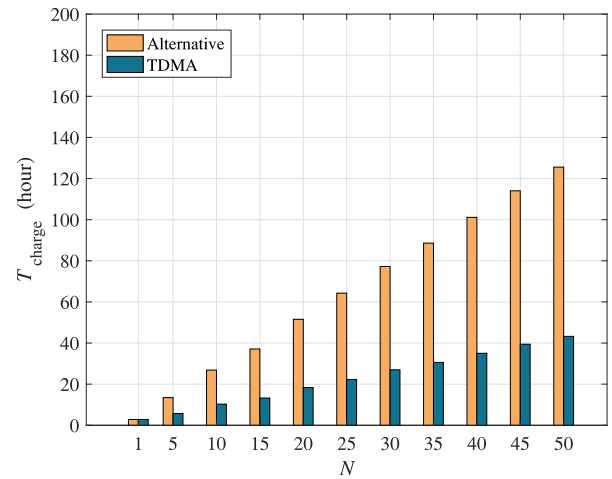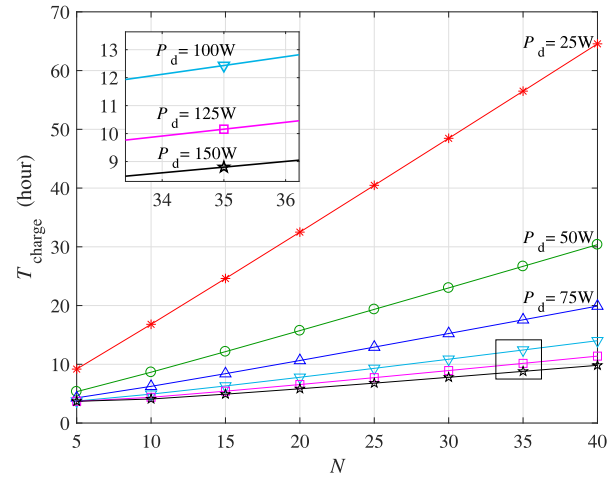

Fig. 12.   Charging time T_{charge} versus receiver number N (0 initial residual battery capacity, TDMA).

obtain the average result. Actually, we have run the simulation for more times and found less distinction on results. As shown in Fig. 11, the T_{charge} of the TDMA scheduling algorithm is almost one third (34.5% when $N = 50$) of that of the alternative scheduling algorithm.

In summary, from Figs. 10 and 11, we find that the efficiency of the TDMA scheduling algorithm is greater than that of the alternative scheduling algorithm.

C. TDMA Charging Algorithm Features

For the alternative scheduling algorithm, the transmitting beam power is dynamic depending on each receiver's requirement. However, for the TDMA scheduling algorithm, the transmitting beam power is fixed. Thus, the driving power P_d is customizable in the TDMA scheduling algorithm, and it can be an desired value. We evaluate here the impacts of the driving power P_d, thus the transmitting beam power with the TDMA scheduling algorithm.

We assume the initial residual capacity is zero. The receiver number N varies from 5 to 40. The driving power P_d is from 25 W to 150 W. In Fig. 12, with the same P_d, T_{charge} increases
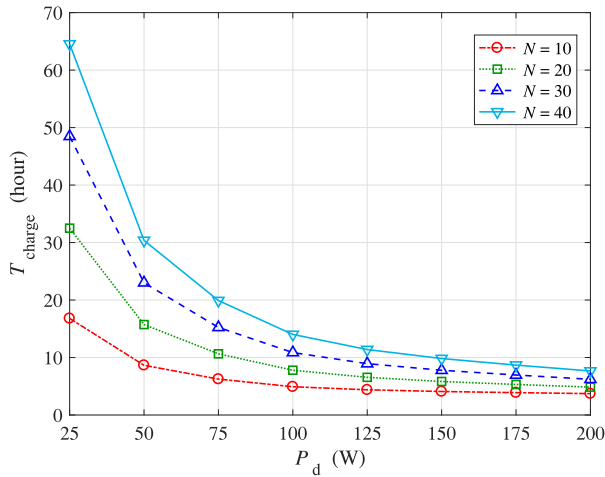
Fig. 13. Charging time T_{charge} versus driving power P_d (0 initial residual battery capacity, TDMA).

Fig. 15. Multiplexing number ψ versus time t (random initial residual battery capacity, Ψ is average multiplexing number, TDMA).
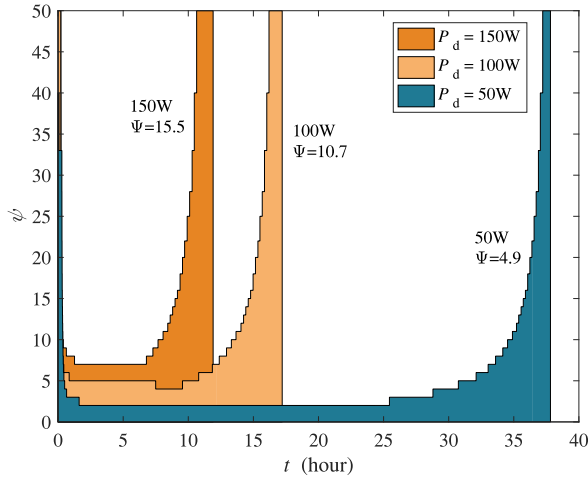

Fig. 14. Multiplexing number ψ versus time t (0 initial residual battery capacity, Ψ is average multiplexing number, TDMA).

almost linearly with N increasing. Moreover, we find out that the slopes of linear lines decline when P_d increasing. For example, the slope of the line for $P_d = 50$ W is about half of that for $P_d = 25$ W.

Fig. 13 illustrates that T_{charge} decreases when P_d increasing for the different receiver number N. However, the impact of the small P_d on T_{charge} is more than that of the large P_d. Furthermore, for the same P_d, T_{charge} increases when N increasing.

Fig. 14 demonstrates the variation of the multiplexing number ψ during the charging period for $N = 50$ receivers. We consider three cases for $P_d = 50$ W, 100 W, and 150 W, respectively. We find that the variation of ψ can be divided into three stages: 1) initially, the ψ is very large; 2) then, it goes down to a very low value and lasts for a long time; and 3) at last, it rises up to a high value again.

The variation pattern of the multiplexing number ψ can be explained by two reasons. The first reason is related to the Li-ion battery charging profile (Fig. 4), i.e., the desired charging power P_c changes from a low level to a high level and then
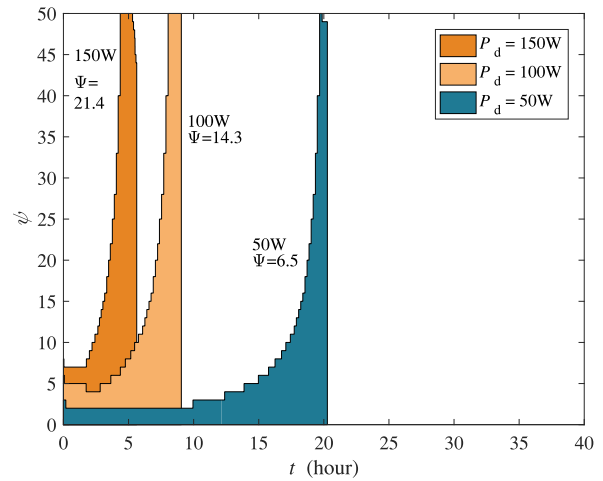
back to the low level during the charging period. Accordingly, the TDMA frame can contain more receivers if the desired charging powers are at the low level. Another reason is that the receivers with 0 initial residual capacity must pass the *low multiplexing number stage*, where P_c is high (see Fig. 4) and one receiver may occupy most slots in the frame.

Similar to Fig. 14, Fig. 15 illustrates the simulation results for the uniformly distributed initial residual capacity. For the same driving power P_d, the average multiplexing numbers Ψ in Fig. 15 are higher than that in Fig. 14.

With random initial residual capacities, it is highly probable that a receiver can be selected for the unallocated slots in the scheduling frame. Therefore, the scheduling frame can multiplex more receivers than the case with zero initial residual capacity. On the other hand, in Fig. 15, due to the random initial residual capacity, some receivers' battery states may be at the tail of its charging profile as in Fig. 4. Thus, the required P_c of these receivers should be low, which may lead to the small N_c. Therefore, the low multiplexing number stage in the middle of the charging period in Fig. 15 is shorter than that in Fig. 14. Moreover, the average multiplexing number Ψ in Fig. 15 is larger than that in Fig. 14.

D. Summary

The TDMA scheduling algorithm has higher efficiency than the alternative scheduling algorithm. For the TDMA scheduling algorithm, the relationship between the charging time T_{charge} and the receiver number N is close to linearity. The relationship between T_{charge} and the driving power P_d as in Fig. 13 provides a guideline for the transmitter design. Moreover, the variation of the multiplexing number ψ reflects the efficiency. Hence, increasing the value of ψ is an important approach to design more efficient TDMA charging schedulers.

VI. CONCLUSION

We propose the TDMA charging design for multiuser WPT in the ARBC system. At first, we present the point-to-point ARBC system; describe multiuser charging problem;

and demonstrate the alternative charging method. Then, we introduce the principle of the TDMA charging in the ARBC system and depict its digitalized implementation. Next, we propose the TDMA-based scheduling algorithm. Finally, we compare the efficiency of the alternative and TDMA scheduling algorithms by simulation. In summary, the TDMA charging enables multiuser WPT with continuous battery charging current. Furthermore, it provides the transmitter with flexible output capability, because the maximum output power has no limitation. The simulation results show that the TDMA scheduling algorithm has high efficiency, as the total charging time is almost half (46.9% when charging 50 receivers) of that of the alternative scheduling algorithm.

In the future, we will investigate the efficiencies of the circuit components and the dynamic property of Li-ion battery. Moreover, flow control and the scheduler with quality of service can be further studied.

Acknowledgment

References

[1] A. Carroll and G. Heiser, "An analysis of power consumption in a smartphone," in *Proc. USENIX Annu. Tech. Conf.*, Boston, MA, USA, 2010, p. 21.

[2] K. Georgiou, S. Xavier-de-Souza, and K. Eder, "The IoT energy challenge: A software perspective," *IEEE Embedded Syst. Lett.*, to be published.

[3] S. Yu, W. Zhou, S. Guo, and M. Guo, "A feasible IP traceback framework through dynamic deterministic packet marking," *IEEE Trans. Comput.*, vol. 65, no. 5, pp. 1418–1427, May 2016.

[4] G. Ding *et al.*, "An amateur drone surveillance system based on the cognitive Internet of Things," *IEEE Commun. Mag.*, vol. 56, no. 1, pp. 29–35, Jan. 2018.

[5] Q. Wu *et al.*, "Cognitive Internet of Things: A new paradigm beyond connection," *IEEE Internet Things J.*, vol. 1, no. 2, pp. 129–143, Apr. 2014.

[6] X. Lu, P. Wang, D. Niyato, D. I. Kim, and Z. Han, "Wireless charging technologies: Fundamentals, standards, and network applications," *IEEE Commun. Surveys Tuts.*, vol. 18, no. 2, pp. 1413–1452, 2nd Quart., 2016.

[7] J. Garnica, R. A. Chinga, and J. Lin, "Wireless power transmission: From far field to near field," *Proc. IEEE*, vol. 101, no. 6, pp. 1321–1331, Jun. 2013.

[8] S. S. Valtchev, E. N. Baikova, and L. R. Jorge, "Electromagnetic field as the wireless transporter of energy," *Facta Universitatis Electron. Energ.*, vol. 25, no. 3, pp. 171–181, Dec. 2012.

[9] S. Assawaworrarit, X. Yu, and S. Fan, "Robust wireless power transfer using a nonlinear parity-time-symmetric circuit," *Nature*, vol. 546, no. 7658, pp. 387–390, Jun. 2017.

[10] B. L. Cannon, J. F. Hoburg, D. D. Stancil, and S. C. Goldstein, "Magnetic resonant coupling as a potential means for wireless power transfer to multiple small receivers," *IEEE Trans. Power Electron.*, vol. 24, no. 7, pp. 1819–1825, Jul. 2009.

[11] K. H. Yi, "High frequency capacitive coupling wireless power transfer using glass dielectric layers," in *Proc. Wireless Power Transf. Conf.*, Aveiro, Portugal, May 2016, pp. 1–3.

[12] N. Shinohara, *Wireless Power Transfer via Radiowaves*. New York, NY, USA: Wiley, 2014.

[13] J. Fakidis, S. Videv, H. Helmers, and H. Haas, "0.5-Gb/s OFDM-based laser data and power transfer using a GaAs photovoltaic cell," *IEEE Photon. Technol. Lett.*, vol. 30, no. 9, pp. 841–844, May 1, 2018.

[14] Q. Liu *et al.*, "Charging unplugged: Will distributed laser charging for mobile wireless power transfer work?" *IEEE Veh. Technol. Mag.*, vol. 11, no. 4, pp. 36–45, Dec. 2016.

[15] Q. Zhang *et al.*, "Adaptive distributed laser charging for efficient wireless power transfer," in *Proc. IEEE 86th Veh. Technol. Conf. (VTC-Fall)*, Toronto, ON, Canada, Sep. 2017, pp. 1–5.

[16] A. Madhja, S. Nikoletseas, and T. P. Raptis, "Distributed wireless power transfer in sensor networks with multiple mobile chargers," *Comput. Netw.*, vol. 80, pp. 89–108, Apr. 2015.

[17] W. Xu, W. Liang, X. Lin, and G. Mao, "Efficient scheduling of multiple mobile chargers for wireless sensor networks," *IEEE Trans. Veh. Technol.*, vol. 65, no. 9, pp. 7670–7683, Sep. 2016.

[18] B. Feng, H. Zhang, H. Zhou, and S. Yu, "Locator/identifier split networking: A promising future Internet architecture," *IEEE Commun. Surveys Tuts.*, vol. 19, no. 4, pp. 2927–2948, 4th Quart., 2017.

[19] E. Gallagher, "A digital PCM time-division switching system," *IEEE Trans. Commun. Technol.*, vol. COM-16, no. 6, pp. 759–770, Dec. 1968.

[20] C. Jiang, K. T. Chau, T. W. Ching, C. Liu, and W. Han, "Time-division multiplexing wireless power transfer for separately excited DC motor drives," *IEEE Trans. Magn.*, vol. 53, no. 11, pp. 1–5, Nov. 2017.

[21] A. J. Forsyth and S. V. Mollov, "Modelling and control of DC–DC converters," *Power Eng. J.*, vol. 12, no. 5, pp. 229–236, Oct. 1998.

[22] W. I. Newman, *Continuum Mechanics in the Earth Sciences*. Cambridge, U.K.: Cambridge Univ. Press, 2012.

[23] W. W. Weaver and P. T. Krein, "Implementing power buffer functionality in a DC–DC converter by geometric control," in *Proc. Conf. Rec. IEEE Ind. Appl. Conf. 41st IAS Annu. Meeting*, Tampa, FL, USA, Oct. 2006, pp. 2529–2536.

[24] S. Dearborn, "Charging Li-ion batteries for maximum run times," *Power Electron. Technol.*, vol. 31, pp. 40–49, Apr. 2005.

[25] Laser Diode Source Control and Medical Technologies. *Laser Diode Source—808nm*. Accessed: Jan. 2018. [Online]. Available: https://www.laserdiodesource.com/shop/808nm-25Watt-Laser-Diode-Module-BWT-Beijing

[26] Q. Zhang *et al.*, "Distributed laser charging: A wireless power transfer approach," *IEEE Internet Things J.*, to be published.

[27] S. A. Salman, J. M. Khalel, and W. H. Abas, "Calculation of the attenuation of infrared laser beam propagation in the atmosphere," *J. Res. Diyala Humanity*, vol. 37, pp. 81–91, 2009.

[28] E. Oliva, F. Dimroth, and A. W. Bett, "GaAs converters for high power densities of laser illumination," *Progr. Photovolt. Res. Appl.*, vol. 16, no. 4, pp. 289–295, Jun. 2008.

[29] R.-J. Wai, C.-Y. Lin, R.-Y. Duan, and Y.-R. Chang, "High-efficiency DC–DC converter with high voltage gain and reduced switch stress," *IEEE Trans. Ind. Electron.*, vol. 54, no. 1, pp. 354–364, Feb. 2007.

[30] Texas Instruments. *TPSM84624 4.5V to 17V Input, 0.6V to 10V Output, 6A Power Module*. Accessed: Jan. 2018. [Online]. Available: http://www.ti.com/lit/ds/symlink/tpsm84624.pdf
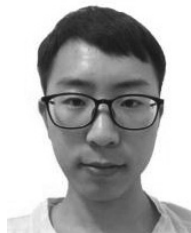
Mingliang Xiong received the B.S. degree in communication engineering from the Nanjing University of Posts and Telecommunications, Nanjing, China, in 2017. He is currently pursuing the Ph.D. degree at the College of Electronics and Information Engineering, Tongji University, Shanghai, China.

His current research interests include wireless power transfer, simultaneous wireless information and power transfer, and the Internet of Things.
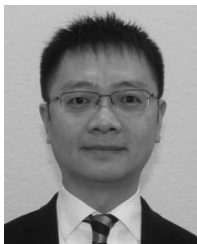
Mingqing Liu received the B.S. degree in computer science and technology from Northwest A&F University, Yangling, China, in 2018. She is currently pursuing the Ph.D. degree at the College of Electronics and Information Engineering, Tongji University, Shanghai, China.

Her current research interests include wireless power transfer, development of remote wireless charging technology, the Internet of Things, and financial transactions.

Qingqing Zhang (S'16) received the M.E. degree in computer science and technology from the Hunan University of Technology, Zhuzhou, China, in 2016. She is currently pursuing the Ph.D. degree at the College of Electronics and Information Engineering, Tongji University, Shanghai, China.

Her current research interests include wireless charge, wireless power transfer, simultaneous wireless information and power transmission, the Internet of Things, and communications.

Jun Wu (M'03–SM'14) received the B.S. degree in information engineering and M.S. degree in communication and electronic systems from Xidian University, Xi'an, China, in 1993 and 1996, respectively, and the Ph.D. degree in signal and information processing from the Beijing University of Posts and Telecommunications, Beijing, China, in 1999.

He was a Principal Scientist with Huawei, Shenzhen, China, and Broadcom, Irvine, CA, USA. In 2010, he joined the College of Electronics and Information Engineering, Tongji University, Shanghai, China, as a Professor. His current research interests include wireless communication, information theory, and multimedia signal processing.

Qingwen Liu (M'07–SM'15) received the B.S. degree in electrical engineering and information science from the University of Science and Technology of China, Hefei, China, in 2001, and the M.S. and Ph.D. degrees from the Department of Electrical and Computer Engineering, University of Minnesota, Minneapolis, MN, USA, in 2003 and 2006, respectively.

He is currently a Professor with the College of Electronics and Information Engineering, Tongji University, Shanghai, China. His current research interests include wireless power transfer and the Internet of Things.

Pengfei Xia received the Ph.D. degree from the Department of Electrical and Computer Engineering, University of Minnesota Twin Cities, Minneapolis, MN, USA, in 2005.

He is currently a Full Chair Professor with the College of Electronics and Information, Tongji University, Shanghai, China. He co-edited *60 GHz Technology for Gb/s WLAN and WPAN: From Theory to Practice* (Wiley, 2010). His current research interests include wireless communications, networks, and signal processing.

Dr. Xia was a co-recipient of the IEEE Signal Processing Society Best Paper Award in 2011. He currently serves as a Signal Processing for Communications (SPCOM) Technical Committee member and SPCOM Industrial/Government Subcommittee Chair for the IEEE Signal Processing Society.